Nano Crystalline Ceramic and Ceramic Coatings Made by Conventional and Solution Plasma Spray

Eric H. Jordan and Maurice Gell

University of Connecticut
Storrs, CT 06269
USA

jordan@engr.uconn.edu

INTRODUCTION

Nanostructured ceramic coatings produced by plasma spray processes are being developed for a wide variety of applications that require resistance to wear, erosion, cracking and spallation [1]. In addition the process is being developed to make near net shaped ceramic performs by dissolution of the substrate after spraying. Attractive properties associated with a nanostructure (in general referring to grain size smaller than 100 nm) have been documented for bulk materials [1–8]. It is anticipated that, if properly deposited, nanostructured ceramic coatings could also provide improved properties for variety of applications, including wear resistant [9, 10] and thermal barrier coatings [11, 12]. Thermal spray techniques are often used to deposit thick oxide coatings and experimental examination of phase constituents, microstructures and mechanical properties with respect to processing conditions have been extensively carried out and reviewed [13–19]. This is one of the first papers that deals with similar studies for nanostructured coatings. In this paper three different applications are discussed. Conventional air plasma spray of nano crystalline alumina-titania ware coatings for ship applications and then liquid precursor spray of nano crystalline thermal barrier coatings for turbine applications finally a brief mention of recent progress in spraying dense materials for use a stand alone ceramics will be presented.

PART I: AIR PLASMA SPRAY OF ALUMINA-TITANIA WARE COATINGS FOR SUBMARINE APPLICATION

1.1 Experimental Procedure

The nanostructured Al_2O_3 and TiO_2 powders employed in this study were obtained from Nanophase Technology Corporation™, Burr Ridge, IL. The powders have a mean diameter of 50 and 70 nm, respectively. These powders were blended to produce a powder mixture with composition equivalent to commercially available Metco-130 (Al_2O_3-13wt.%TiO_2). In addition, small amounts of nanostructured oxide powders were added during mixing for a modified nanostructured powder. The mixed powders were then reconstituted to form micrometer-size agglomerates (40–70 mm) that are large enough to be used commercial powder feeders. The process of reconstitution consists of spray drying a slurry containing nano-alumina and nano-titania particles and subsequent heat treatment at high temperature (800–1200°C). Plasma reprocessing of the powders was carried out for the modified powders. Characterization of the reconstituted agglomerates, as well as Metco-130 powders, were carried out by X-ray diffraction (XRD) and electron microscopy for phase identification and examination of agglomerate size, shape, morphology and microstructure. Plasma spray of the reconstituted agglomerates and Metco-130 powders was carried out with a Metco 9 MB plasma

torch and GH nozzle. The coatings were deposited up to 300 mm thick on mild carbon steel substrates of various geometries specifically designed for specific mechanical property tests. The plasma spray of oxide coatings in this study was carried out as a function of a critical plasma spray parameter (CPSP) defined as [9]:

CPSP= Voltage*Current/ Primary Gas (Ar) Flow Rate

(1) Other processing variables such as carrier gas flow rate, spray distance, flow rate ratio of Argon to H2, powder feed rate, gun speed, etc., were held constant in this study. Under these controlled processing conditions, CPSP can be directly related to the temperature of the plasma and/or the particles [20]. The alumina-titania coatings deposited by plasma spraying at various CPSP values are summarized in Table 1.

**Table 1: Specimen designation for plasma sprayed alumina-titania
coatings and the corresponding CPSP values**

CPSP	Commercial coating Metco-130	Nano-alumina–titania	Modified nano-alumina–titania*
270	–	S270	–
300	C300	S300	M300
325	C325	S325	M325
350	–	–	M350
390	–	–	M390
410	C410	–	M410

* Modified with small amounts of other additives.

For each specific CPSP condition, a total of 20 specimens were plasma sprayed concurrently using an apparatus that held all 20 mild steel substrates (approximately 2 mm in thickness). Among these 20 specimens, four coupons (2.54 cm in diameter) were coated for modified ASTM-C633-79 direct pull-test [21], four coupons (2.54 cm in diameter) for abrasive wear test, four plates (5X5 cm) for cup test, four plates (6X5 cm) for bend test and four plates (5X5 cm) for sliding wear test. Schematic illustrations of the cup test and the bend test are presented in Fig. 1 and the detailed description of the direct-pull test, abrasive wear test and sliding wear test are given elsewhere [9,10,21].
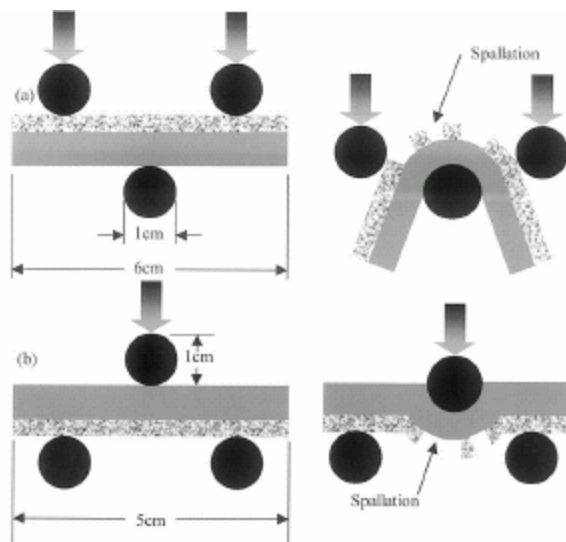
**Figure 1: Schematic illustrations for (a) bend and (b) cup tests
carried out for plasma sprayed alumina-titania coatings.**

Also, microhardness and indentation crack growth resistance of the coatings were measured using Vickers indentation technique (HV300 and HV3000, respectively) and the amount of porosity in the coatings were estimated from electron micrographs by quantitative image analysis. In addition, constituent phases were characterized by XRD and an estimate of the volume fraction of microstructural features that developed during the plasma spray was performed using quantitative image analysis.

1.2   Properties of Plasma Sprayed Coatings

Physical and mechanical properties, including density, hardness, indentation crack growth resistance, adhesive strength, spallation resistance in bend and cup-tests, and resistance to abrasive and sliding wear, of the plasma sprayed coatings were evaluated. These properties were also examined as a function of CPSP and compared with the Metco-130 coatings. Based on quantitative image analysis, the amount of porosity was evaluated for three coating systems as a function of CPSP, as shown in Fig. 2.
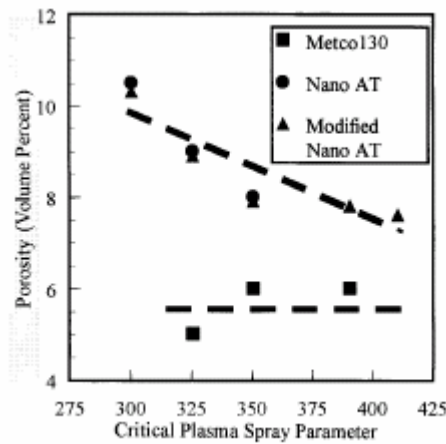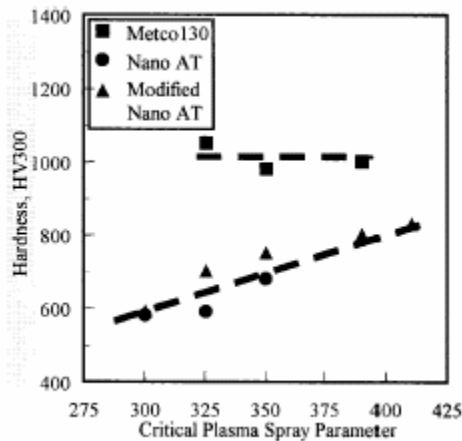


Figure 2: Porosity decreases with CPSP.

A decrease in porosity was observed for both nanostructured and modified-nanostructured alumina-titania coatings with an increase in the CPSP. No variation was observed for Metco-130. In Fig. 3, the indentation hardness (HV300) for the three coatings as a function of CPSP is presented.

Figure 3: Hardness vs. critical plasma spray parameter (CPSP).

While no variation was observed for Metco-130 coatings, an increase in hardness was observed for nanostructured coatings Indentation crack growth resistance of the coatings was also estimated by measuring the length of the two horizontal cracks originating from the corners of the Vickers indentation. A maximum value in the indentation crack growth resistance was observed for nanostructured alumina-titania coatings at an intermediate CPSP (:350) as shown in Fig. 4.
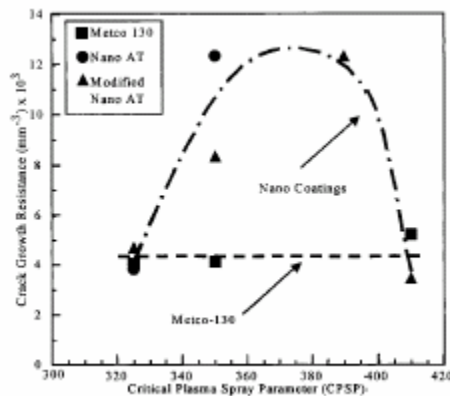
Figure 4: Crack growth resistance vs. CPSP showing superior toughness of the nano coatings.

The indentation crack growth resistance of the Metco-130 coatings remain the same as a function of CPSP. Alumina-titania coatings, plasma sprayed on plate (6X5 cm) substrates, were subjected to bend and cup test, as schematically illustrated in Fig. 1. For each coating type and CPSP, four specimens were tested. Based on visual inspection, the coatings in the bend test were categorized into three groups, (a) complete failure; (b) partial failure and (c) pass. Representative photographs of these results are presented in Fig. 5.
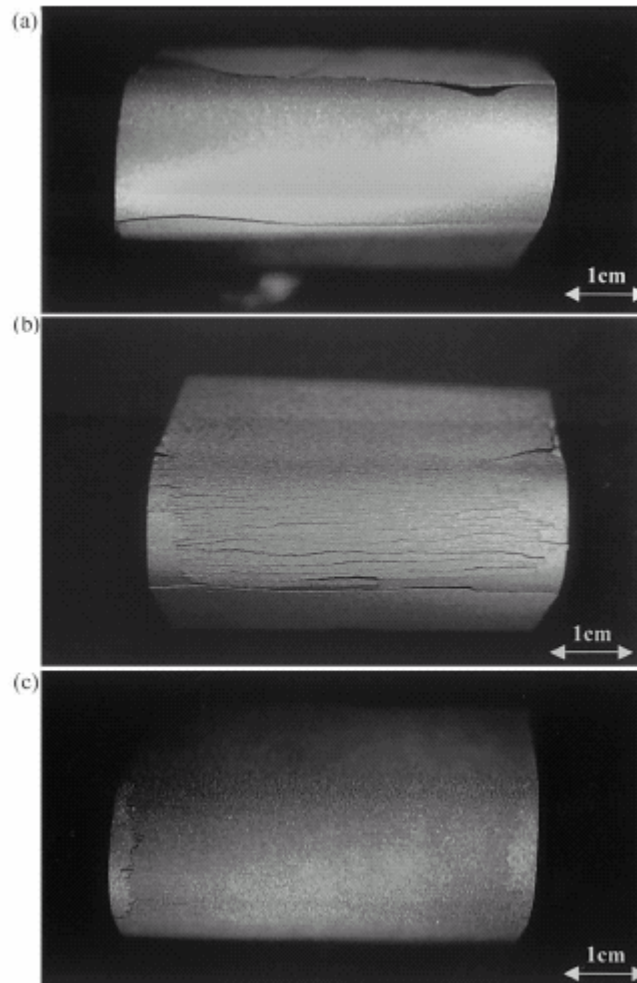
**Figure 5: (a) Complete failure (b) partial failure (c) pass. Completed failure was observed for
Metco 130 while partial or no failure was observed for nanostructured aluminia-titania.**

Significant spallation, identified as complete failure, was observed for all Metco-130 coatings. However, for nanostructured alumina-titania coatings, partial failure and pass were observed as reported in Table 3. The nanostructured coatings were resistant to bend-failure at lower CPSP. The coatings exhibited similar behavior in cup-tests. While Metco-130 coatings exhibited significant cracking and spallation as shown in Fig. 6a, only minimum spallation was observed without cracking for nanostructure alumina-titania coatings as shown in Fig. 6b.
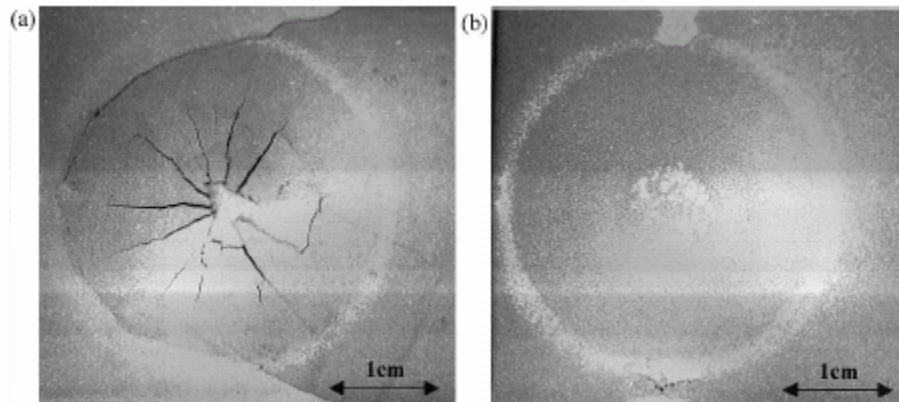
Figure 6: Behavior in cup bulge tests (a) Metco 130 (b) nanostructure aluminia-titania.

Adhesive strength of the coatings was measured using the modified ASTM direct-pull test [21]. Significant improvement (\2 X) was observed for nanostructured coatings deposited at selected CPSP's compared with Metco-130 deposited according to manufacturer's recommendation, e.g. CPSP_410, as shown in Fig. 7.
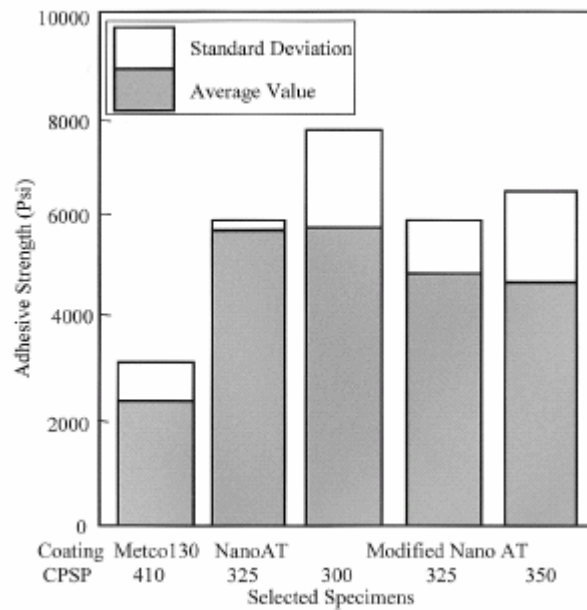
Figure 7: Adhesive strength of coatings showing improved strength of nanostructured coatings.

The value of the adhesion strength for the Metco-130 agreed with that specified by the manufacturer [23]. Improvements in the abrasive wear resistance were also observed for nanostructured coatings deposited at selected CPSP's as shown in Fig. 8.
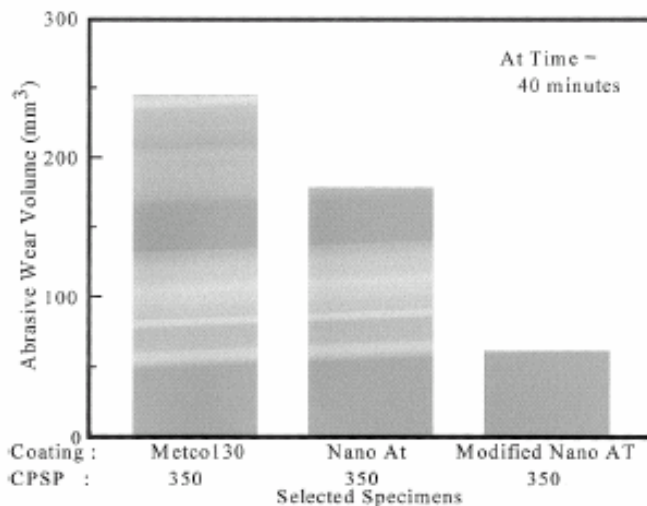
**Figure 8: Abrasive wear volume losses showing improved
wear properties for nanostructured coatings.**

Such findings are consistent with previous results where the corresponding wear mechanisms were proposed [10]. Improvement in sliding wear resistance was also observed for nanostructured coatings; consistent with previous results [9]. Details of the results and the associated mechanism related to the improved sliding wear resistance of the nanostructured coatings are currently under investigation. Typical results from a 'scratch-test' using a diamond indentorshow that for nanostructured coatings, the wear track has a small width and a minimum extrusion of materials. For Metco- 130 coatings, the wear track is wider with more debris. These observations from 'scratch-tests' support the improved abrasive and sliding wear resistance realized by nanostructured alumina-titania coatings deposited by plasma spray process at appropriate CPSP. Heat treatment at high temperature (800–1200°C) produces the equilibrium phase for both Al2O3 and TiO2 (e.g. a-Al2O3 and rutile-TiO2). However, for modified nanostructured Al2O3-13wt.%TiO2, plasma-reprocessing after the heat treatment yields the non-equilibrium phase of TiO2. The disappearance of the rutile-TiO2 phase indicates that melting has occurred during the plasma-reprocessing of the heat-treated powders. Thus, the presence of equilibrium a-Al2O3 and non-equilibrium anatase-TiO2 may arise following the plasma reprocessing from an air-quench that is rapid enough to form anatase–TiO2. Variation in the microstructure, ranging from dendritic-solidification structure to partially-molten (i.e. liquid phase sintered) morphology was observed for the modified nano-agglomerates. This inhomogeniety may be due to the variation in particle size and thermal history that individual particles experience during plasma reprocessing. Fo plasma sprayed alumina-titania coatings, only a-Al2O3 and g-Al2O3 phases were found and TiO2 phases were absent. Since the solubility of TiO2 in the equilibrium alpha-Al2O3 is negligible, Ti ions are likely to be in the gamma-Al2O3 lattice as either an interstitial or substitutional defect. Formation of non-equilibrium g- Al2O3 for plasma sprayed pure alumina coatings has been extensively reviewed by McPherson [14,15]. Recent XRD investigation by Kear et al. [24], suggests that the plasma sprayed Al2O3-13wt.%TiO2 coatings contain non-equilibrium x-phase-Al2O3 · TiO2 phase in which Ti ions randomly occupy the Al lattice sites in the g-Al_2O_3 structure. The peak positions of XRD for x-Al2O3 · TiO2 phase are identical to those of g-Al2O3, however the relative intensity of peaks are different [24]. The formation of x-Al2O3 · TiO2 phase must originate from rapid liquid-to-solid transformation, which is expected during the plasma spray process and provides reasonable explanation for the absence of Ti-containing phase. The non-equilibrium phase observed in this study can be identified as the x-Al2O3 · TiO2 phase [24] by virtue of having the appropriate position and

intensity of XRD peaks. Thus, the plasma sprayed nanostructured alumina-titania coatings consist of equilibrium a-Al2O3 and non-equilibrium x-Al2O3 · TiO2 phase.

1.3   Mechanical Properties and Critical Plasma Spray Parameter

Various properties, including porosity, hardness, indentation crack growth resistance, bend-test, cup-test, adhesive strength, abrasive and sliding wear resistance were evaluated for plasma sprayed alumina-titania coatings. The results, presented in Fig. 3 through 8, indicate that improvements in indentation crack growth resistance, resistance to cracking and spallation, adhesion strength, resistance to abrasive and sliding wear were observed for the nanostructured alumina-titania coatings, despite higher porosity and lower hardness. In addition, improvements in some properties were found at intermediate values of CPSP, for which partial melting of reconstituted agglomerates introduce sub-micron a-Al2O3. Further improvement in the modified Al2O3- 13wt.%TiO2 may be associated with chemistry as well as further reduction in grain size. In this study, nano-coatings outperformed conventional coatings in cup and bend tests and the test results improved as the amount of PM microstructure increased and CPSP decreased as indicated in Figs. 5 and 6 and as reported in Table 3. Improvement in cup and bend test would be expected if the cracking perpendicular to the coatings:substrate interface occurs more easily than the spallation-debonding. Thus, the improved adhesive strength of nano-derived coatings would be expected to give improved cup and bend test results. Fig. 10 shows that the indentation crack growth resistance peaks at spray parameters of CPSP between 350 and 380. These results can be associated with a microstructural mixture having both FM and PM regions. It is further worth noting that the indentation cracking was almost exclusively parallel to the metal ceramic interface and many of the cracks are more than ten indentation diagonals long. It is likely that cracks extending so far from the indentation are influenced not only by the splat boundary weakness but also by residual stresses within the coating. Detailed studies on this issue are currently under way. It is interesting to consider the relation between the improved mechanical properties and the observed microstructure. All the coatings deposited from the reconstituted nanostructured agglomerates had improved adhesive strength. Interestingly, the improvement in adhesive strength occurred regardless of the spray conditions or the fraction of the microstructure that was PM or even the presence of modifying elements as indicated in Fig. 13. During the adhesive strength test of nano-derived coatings, failures almost always occurred within the coating near the coating:substrate interface; thus the adhesive strength for the nanoderived coatings may be governed by the tensile strength of the nanostructured coatings. On the other hand, the Metco 130 coatings were the only coatings to show a significant fraction of failures at the ceramic to metal interface. The reason for the approximate doubling of the adhesive strength is not clear from the present study and is now being actively investigated with attention being paid to the higher purity chemistry and more uniform microstructure of the nano-materials.

1.4   Conclusions Part I

Nanostructured alumina-titania coatings were produced by plasma spray of reconstituted nanostructured powders, using optimized processes, defined by a critical plasma spray parameter. Superior mechanical properties were achieved including indentation crack resistance, adhesion strength, spallation resistance against bend- and cup-test, abrasive wear resistance, sliding wear resistance. As a result a variety of ship related parts have been successfully coated Figure 9 and are in use. The superior properties are associated with coatings that have a retained nanostructure, especially with partial melting of the nanostructured powders.

Shipboard and Submarine Applications for U.S. Navy

Front & Aft Door Support
Front & Aft Arm
Periscope Piston Rod

Figure 9: Example Parts Coated using the Nanostructure Plasma Sprayed material.

PART II: SOLUTION PRECURSOR PLASMA SPRAY OF THERMAL BARRIER COATINGS

2.1   Introduction

Gas turbine hot section components are subjected to hot gasses with temperatures exceeding the melting temperature of the alloys from which they are made. As a result hot part designs include critically important features to reduce metal temperatures which include internal and film cooling and the application of ceramic insulating thermal barrier coatings (TBCs).

Current thermal barrier coatings are ceramic insulating layers, which are deposited on the metallic component to reduce metal temperatures by as much as 150 ºC. The extensive literature on the properties and failure behavior of such coatings can be found in several recent reviews [25]. Current production coatings are made predominantly of 7% Y_2O_3 stabilized ZrO_2 . These coatings are made either by air plasma spray (APS) or deposited by electron beam physical vapor deposition (EB-PVD). In general EB-PVD coatings have superior durability but have higher thermal conductivity and higher cost compared to APS coatings.

In the present paper a third method of making TBC's is presented where the motivation for developing another processing method is to provide an improved combination of properties compared to current practice. The novel method is based on the injection of liquid chemical precursors into a plasma jet forming a ceramic by pyrolosis in the plasma jet. Synthesis of powder materials by similar processes has been carried out for a variety of materials [27] and coatings have been made by related processes for other material systems [28-30]. In our earlier publications various aspects of the production of TBCs by the SPPS process has been presented [31-32]. In the present paper, we seek to provide an updated overview of the work to date with emphasis on the performance of the coatings and the related microstructure and deposition mechanisms.

2.2   Description of the Process

Figure 10 shows the basic configuration for the solution precursor plasma spray process (SPPS). In this process an aqueous solution of the constituent metal salts (Zr and Y) is atomized and injected into a DC arc plasma jet. The ceramic is formed by pyrolosis in the plasma jet prior to reaching the target material or in

some cases after reaching the surface. This spray method is identical to APS deposition with the substitution of a solution atomizer for the solid powder feeder. The atomization can be varied but it involves initial droplet sizes between 20 and 50 microns at various velocities up to 100 m/s [32]. Gun operating powers and gas flows are over the same range as used in making APS coatings.
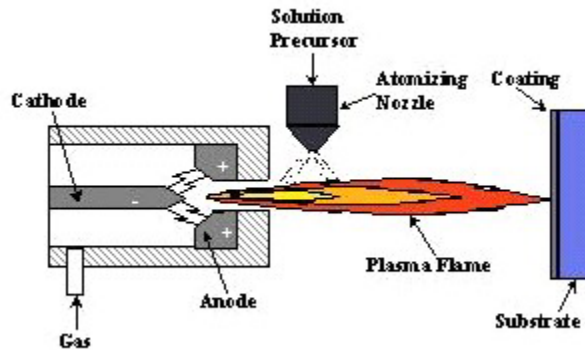

Figure 10: Spray geometry for the solution precursor plasma spray process.

2.3   Experimental Methods

All SPPS coatings shown were made using a Metco 9MB spray system with a 3MB gas-handling panel. The primary gas used was argon and the secondary gas was hydrogen. A custom made fluid delivery system that consists of a precursor storage tank with a regulated nitrogen over pressure that drives fluid flow through a hose that lead to the gas atomizing nozzle mounted at 90 degrees from the gun axis. Nitrogen was used as an atomizing gas. Coating cross sections were made by sectioning the sample on a diamond saw and mounting the samples in epoxy. Following mounting, the samples were polished using standard methods, ending with polishing using a 0.05-micron alumina paste. Samples were examined in a Phillips environmental scanning electron microscope or with a (brand name) FSEM. Sections made to reveal ultra-fine splats were made by first notching the sample with a diamond saw and fracturing them in bending. This is necessary because simple fracture leads to fracture at the vertical cracks revealing a non-typical microstructure. Cyclic furnace durability tests were run in an elevator furnace. The cycle used consisted of a 10 minute heat up, a 40 minute hold at the maximum temperature and 5 minutes of forced air cooling.

2.4   Major Microstructural Features

The microstructure of a typical SPPS coating optimized for use as a TBC is shown in figure 2 along with microstructures from an EB-PVD, a DVC and an APS TBCs for comparison. There are four important microstructural features in SPPS coatings, 1. The deposited ceramic is t' tetragonal phase [32] 2.There are vertical through thickness cracks (Figure 11, 12) . An ultra-fine splat morphology (Figure 3 and 4) 5. micron nanometer size interconnected porosity (Figure 4). This microstructure is different from EB-PVD microstructures where the coating has columnar grains with inter-columnar porosity and from APS coatings, which has a course splat microstructure with prominent transverse splat boundaries (Fig. 12). The microstructure differs form DVC which requires a higher ceramic density (>88%) to produce through-thickness cracks.
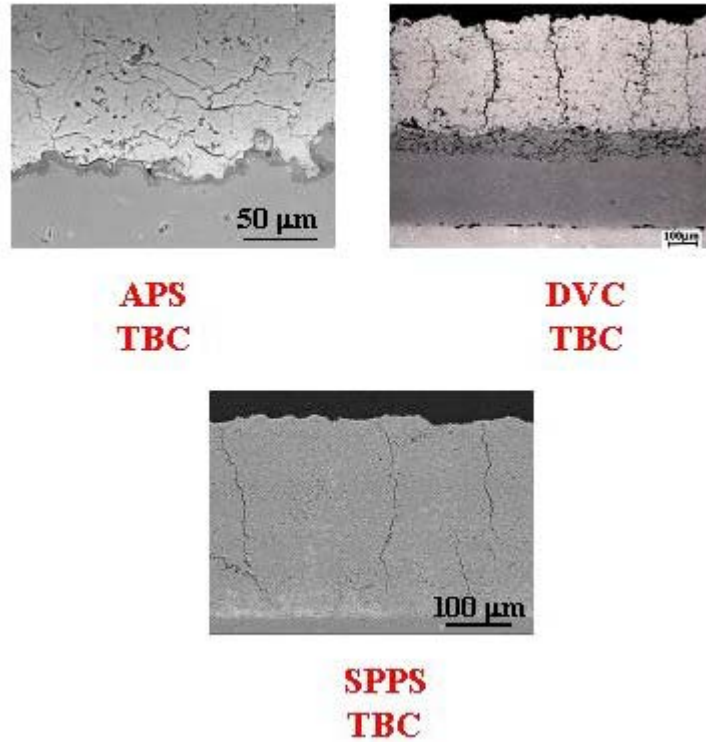
Figure 11: Comparison of SPPS coatings with an EB-PVD coating and an APS coating.
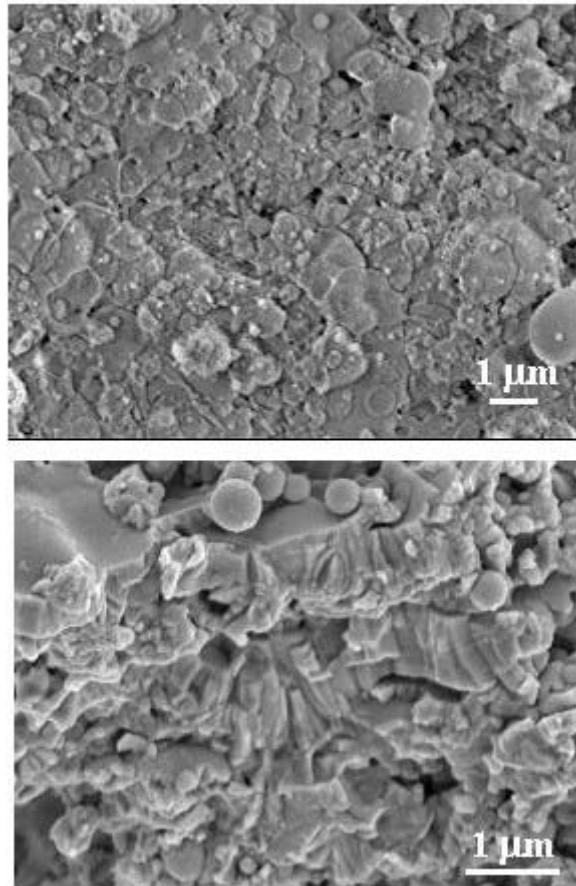
Figure 12: Cross-section of APPS coatings showing ultra-fine splat structures.
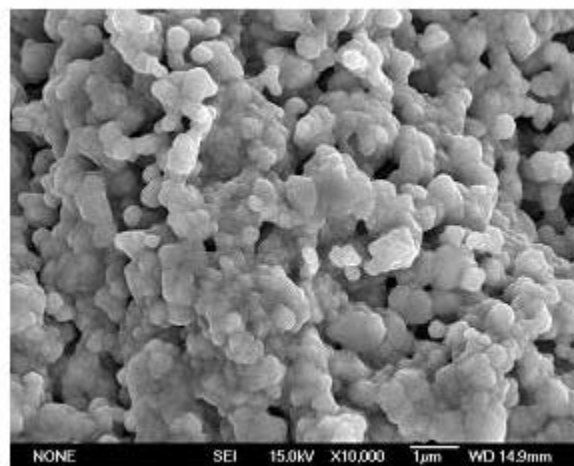

Figure 13: Fracture surface of an SPPS coating showing interconnected porosity.

2.5 TBC Performance

The three most important desirable properties for TBC's is to have:1. a large number of cycle to failure 2. low thermal conductivity 3.a low cost. In assessing these properties 25 mm samples on bond coated substrates were used with the composition as follows:

Table 2

Material Layer	Composition in wt %
SPPS TBC top coat	ZrO2 7-Y2O3
APS Bond coat	
Cast Base alloy	

Cyclic furnace test were performance using 1-hour cycles with a maximum cycle temperature of 1121 °C. The same furnace and temperature cycle have has been used in our previous research programs providing a comparison data base which includes approximately 10 variants (APS and EB-PVD) of bill of material coating systems provided by engine and coating manufacturers. The life of the SPPS coated samples is shown in Figure 14 along with spallation lives of a typical EB-PVD, DVC and APS sample tested in the same rig. The SPPS mean life is the longest we have ever obtained in this test and is 2.5X that of the APS coating and 1.5X that of the EB-PVD coating.
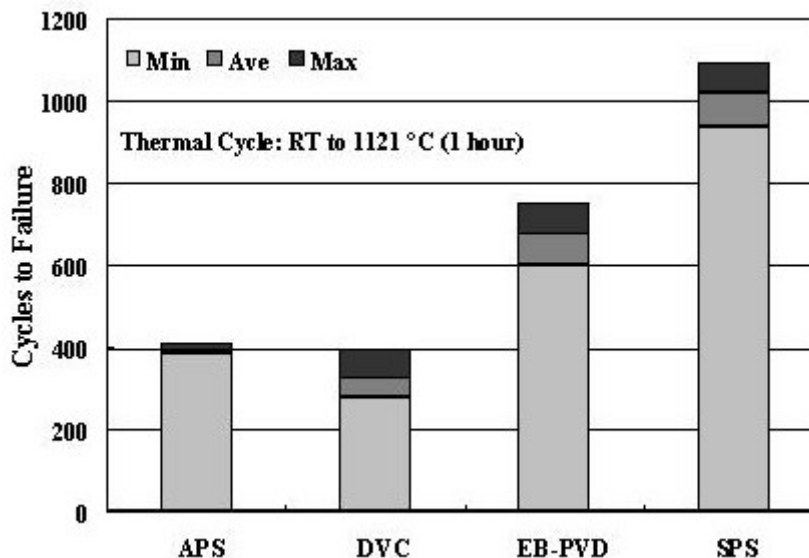

**Figure 14: Comparison of the cyclic life of SPPS coatings and other commercial
coating tested with a maximum cycle temperature of 1121 ºC.**

Figure 15 shows the failure mode for the SPPS coating compared with that of the APS and DVC coatings. In the all three cases, crack initiation and propagation are predominantly in the ceramic just above the TGO to

ceramic interface. Thus, the SPPS coatings are still susceptible to similar failure mechanisms as other plasma sprayed coatings, but such processes take longer for SPPS coatings.
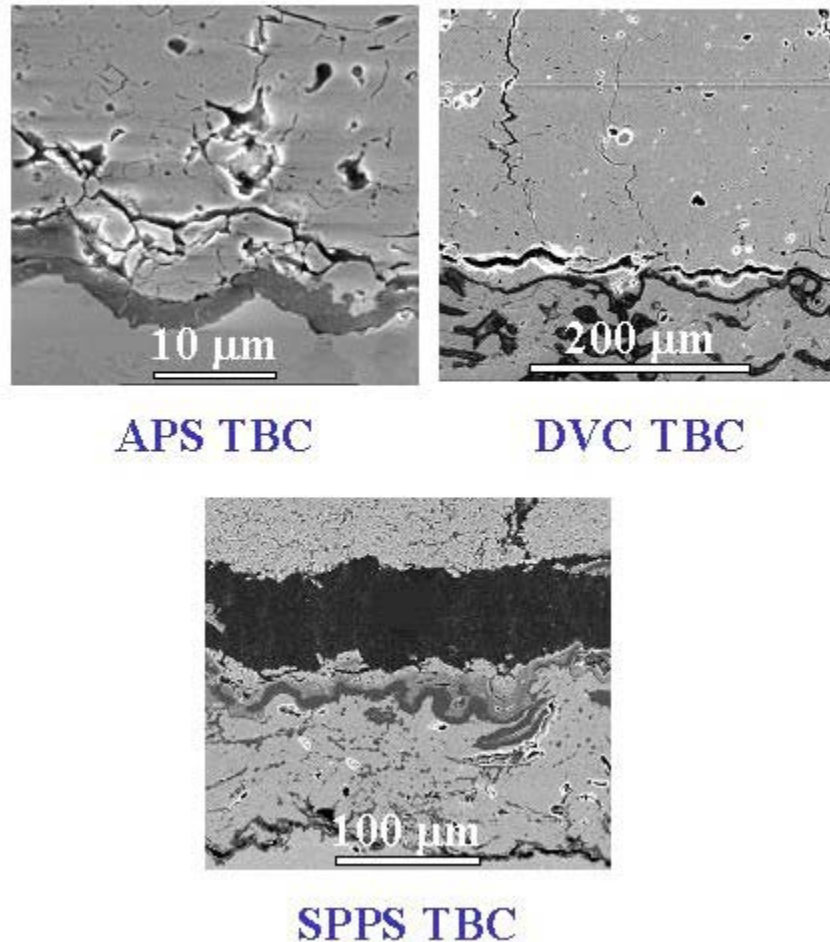
Figure 15: Cross-sections of SPPS, APS and DVC coatings showing similar failure paths.

Thermal conductivity determines the level of thermal protection for a given coating thickness. Figure 16 shows the thermal conductivity measured using the laser flash method vs. temperature for several SPPS coating. The conductivities typical of EB-PVD coatings and APS coatings are show in the figure for comparison. The SPPS coating has lower conductivity than EB-PVD coatings and in the upper part of the range found in APS coatings in its base condition. Also shown is the reduced conductivity produced by structuring the porosity in layers which is done by careful processing and is referred to as inter pass foundries. We have also produced a coating using the advance composition in reference which without inter pass boundaries is similar to the conventional coating with inter pass boundaries shown in Figure 16. We expect the combination of advanced composition and inter pass boundaries to allow 30% lower conductivity than the best standard APS coatings.
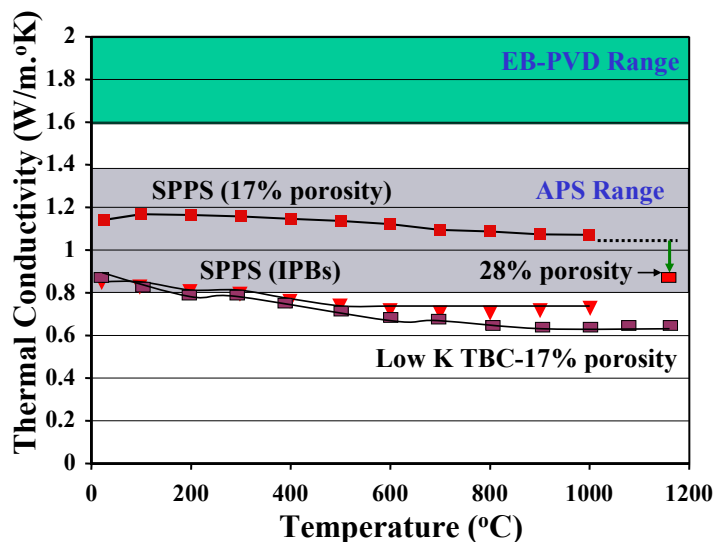
Thermal Conductivity Of SPPS TBCs

Figure 16: Thermal conductivity of SPPS coatings showing improvements due to inter pass boundaries and using a Low K composition combination of both should be even lower.

The cost of making coatings is important. In the case of APS and EB-PVD coatings is well established, as they are industrial processes. The coast of making SPPS coatings can only be estimated based on current practice and deposition rates. A cost analysis was done accounting for the utilization cost of the faculties, material costs, operator cost and deposition rate. Based on this analysis the SPPS coatings are expected to be much less costly than EB-PVD coatings and similar but slightly higher in cost than APS coatings.

Finally in some applications the production of thick coatings is desirable. Because of low deposition rate the production of very thick EB-PVD coatings is not practical. With careful attention to residual stress build up thick APS coating can be produced. In the case of SPPS coatings, thick coatings can be made without any special processing other than coating for a longer time. A 2.5 mm thick coating is show in Figure 17. Interestingly the vertical crack spacing scales with the coating thickness such that the aspect ratio of the regions between the cracks remains roughly constant with a coating thickness to crack spacing typically around 2.
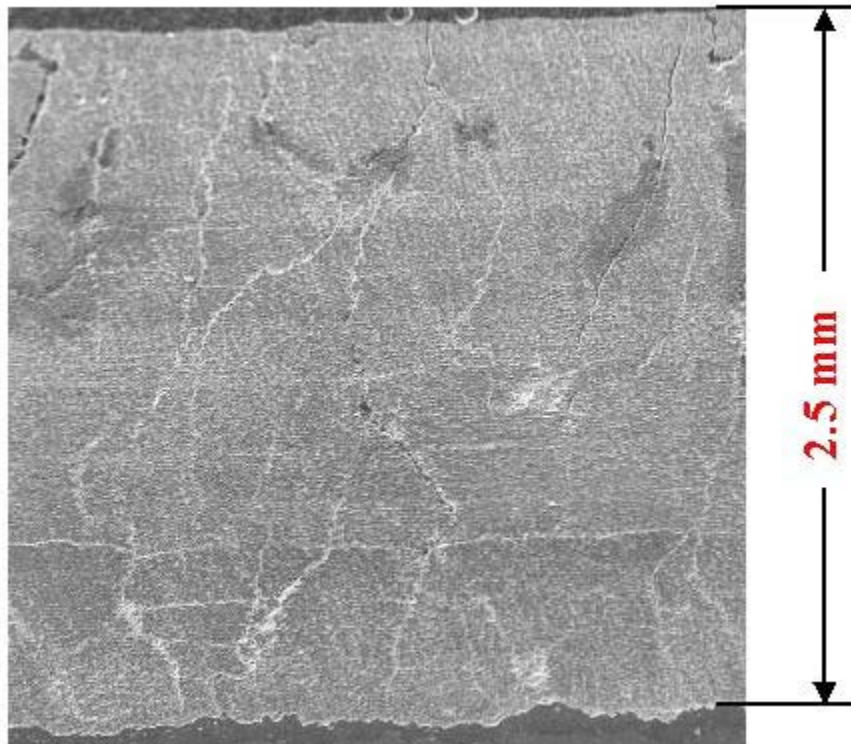
Figure 17: Thick SPPS deposit cross-section.

PART III: MAKING DENSE CERAMICS BY THE SPPS PROCESS

A new effort has been started to make dense ceramic near net shape parts using the SPPS process. This will exploit the ability to make thick ceramics by thermal spray that is one of the characteristics of the SPPS process. The key to making denser ceramics is to get the precursor uniformly and well entrained near the centerline of the plasma jet. This results in fine fully melted materials being deposited. To do this the injection system is being reengineered to have as small a footprint as possible on the plasma jet and as uniform a droplet momentum as possible. By making these changes the Yitriria stabilized Zerconia coating previously having a hardness of 500-600 BHN now have hardness of 1000 BHN. Figure 18 shows the cross section of one such coating. The coating has no vertical cracks as in TBC because there is little to no unpyrolized material being deposited. The residual porosity is believed to be due to the small percentage of large droplets that are generated by the current droplet maker and which arrive with residual water. Efforts to produce sprays which do not have such large droplets are now underway and are expected to yield an even denser but still hard coating. Such coatings will provide a foundation for a spray to shape method of making ceramic parts.
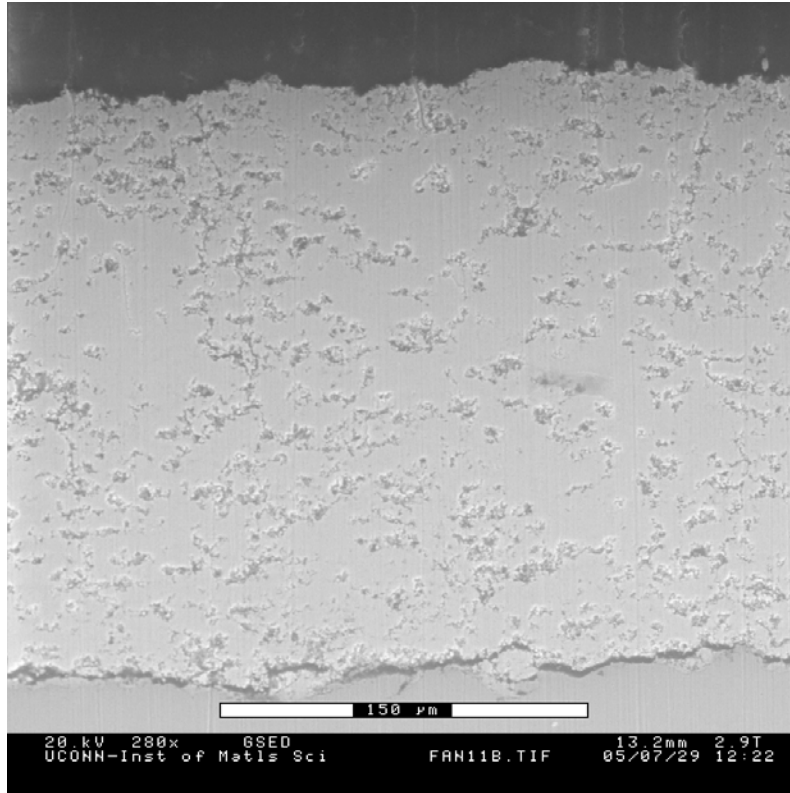
**Figure 18: High hardness (1000 BHN) YSZ coating with
no vertical cracks made by the SPPS process.**

In summary SPPS coatings have superior durability, lower coast and lower thermal conductivity and greater practical thickness limits compared to EB-PVD. Compared to APS coatings, SPPS coatings have superior durability, with comparable but slightly higher cost and thermal conductivity.

REFERENCES

[1]   B. Kear, L.E. Cross, J.E. Keem, R.W. Siegel, F.A. Spaepen, K.C. Taylor, E.L. Thomas, K.N. Tu, Research Opportunities for Materials with Ultrafine Microstructure, National Materials Advisory Board, National Academy Press, Washington, DC, 1989.

[2]   H. Gleiter, Nanostruct. Mater. 1 (1992) 1.

[3]   H. Hahn, Nanostruct. Mater. 2 (1993) 251.

[4]   R.W. Siegel, Nanophase materials: synthesis, structure and properties, in: F.E. Fujita (Ed.), Physics of New Materials, Spinger Heidelberg, 1992.

[5]   R.S. Mishra, C.E. Lesher, A.K. Mukherjee, Mater. Sci. Forum 225–227 (1996) 617.

[6]   R.W. Siegel, Mater. Sci. Forum 235–238 (1997) 851.

[7] K. Jia, T.E. Fischer, Wear 200 (1996) 206.

[8] K. Jia, T.E. Fischer, Wear 203–204 (1997) 310.

[9] L. Shaw, D. Goberman, R. Ren, M. Gell, S. Jiang, Y. Wang, T.D. Xiao, P.R. Strutt, Surf. Coat. Technol., 130 (2000), 1

[10] Y. Wang, S. Jiang, M. Wang, S. Wang, T.D. Xiao, P.R. Strutt, Wear, 37 (2000), 176

[11] M. Gell, J. Met., 46 (1994) 30.

[12] M. Gell, Mater. Sci. Eng. A204 (1995) 246.

[13] R. McPherson, J. Mater. Sci. 15 (1980) 3141.

[14] R. McPherson, J. Mater. Sci. 8 (1973) 851.

[15] R. McPherson, B.V. Shafer, Thin Solid Films 97 (1982) 201.

[16] I.A. Fisher, Int. Metall. Rev. 17 (1972) 117.

[17] T.R. Marlow, C.C. Koch, Mater. Sci. Forum 225–227 (1996) 595.

[18] L. Pawlowski, Surf. Coat. Technol. 31 (1987) 103.

[19] V. Wilms, H. Herman, Thin Solid Films 39 (1976) 251.

[20] S.Y. Semenov, B. Cetegen, unpublished research.

[21] L. Shaw, B. Barber, E.H. Jordan, M. Gell, Scr. Mater. 39 (1998) 1427.

[22] S.A. Saltykov, Streometric Metallography, second ed., Metallurgizdatnd, Moscow, 1958.

[23] Product Bulletin, Sulzer-Metco Corporation.

[24] B.H. Kear, Z. Kalman, R.K. Sadangi, G. Skandan, J. Colaizzi, W.E. Mayo, unpublished research.

[25] Padture, N. Gell, M and Jordan E. H," Thermal Barrier Coatings For Gas-Turbine Engine Applications," Science 296(5566), 280, April 12, (2002).

[26] Evans AG, Mumm Dr, Hutchison JW, Meier, GH and Pettit, FS, " Mechanisms Controlling the Durability of Thermal Barrier Coatings, Prog. Mat. Sci. 46(5), 505-553, (2001).

[27] M. Boulos and E. Pfender," Materials processing with thermal plasmas," MRS Bul. 21 65, (1996)

[28] J. Karthikeyan, C. C. Berndt, S. Reddy, J-Y Wang, A. H. King, and H. Herman, "Nanomaterial deposits formed by DC plasma spraying of liquid feedstocks," J. Am. Ceram. Soc. 81, 121, (1998)

[29] S. D. Parkukuttyamma, J. Margolis, H. Liu, C. P. Grey,S. Sampath, H. Herman, J. B. Parise, "Yttrium aluminum garnet (YAG) films through a precursor plasma spraying technique," J. Am. Ceram. Soc., 84, 1906, (2001)

[30] E. Bouyer, G. Schiller, M. Muller and R. H. Henne, "Characterization of SiC and Si3N4 coatings synthesized by means of inductive thermal plasma from disilane precursors," Appl. Oganomet. Chem. 15, 833, (2001).

[31] Padture, N.P, K.W. Schlichting, T. Bhatia, A. Ozturk, B. Cetegen, E.H.Jordan, M. Gell, S. Jiang, T.D. Xiao, P.R. Strutt, E. Garcia, P. Miranzo and M.I. Osendi." Towards Durable Thermal Barrier Coatings with Novel MicrostructresDeposited by Solution-Precursor Plasma Spray" Acta Mater. 49, 2251, (2001).

[32] Tania Bhatia, Alper Ozturk, Liangde Xie, Eric Jordan, Baki Cetegen, Maurice Gell, Xinqin Ma, Nitin Padture "Mechanisms of Ceramic Coating Deposition in Solution-Precursor Plasma Spray," J. Mater. Res. 17(9), 2363, (2002).